Multiple-Symbol Noncoherent Decoding of Uncoded and Convolutionally Coded Continuous Phase Modulation *

Dan Raphaeli
Electrical Engineering - Systems
Tel Aviv University
Tel Aviv, 69978
Israel

Dariush Divsalar
Jet Propulsion Laboratory 238–420
4800 Oak Grove Dr. Pasadena, CA 91109

September 29, 1999

Abstract

Recently, a method for combined noncoherent detection and decoding of trellis-codes (noncoherent coded modulation) has been proposed, which can practically approach the performance of coherent detection. Here, we successfully apply the technique to the detection of Continuous Phase Modulation (CPM), coded or uncoded. Both full and partial response CPM schemes with arbitrary modulation index are considered. This method is based on multiple-symbol observations, such that the observations are time-overlapped. The results show that most CPM schemes require short observations to achieve almost the same power efficiency as optimally detected coherent CPM. Compared to the previously proposed methods for noncoherent detection that can approach the coherent performance, the required observation length is much shorter and also the decoding complexity is much lower. A new trellis diagram for noncoherent CPM is suggested for simplifying the analysis and the decoder structure. The error performance for uncoded CPM is evaluated by using the union bound technique applied on the symbol-difference trellis diagram. For the coded case a pair-state trellis is required. Very efficient sub-optimal decoding algorithms with very small degradation may implement the non-coherent decoder. The performance achieved with these algorithms is demonstrated by simulations.

*This paper was presented in part at the 1994 Communication Theory Mini Conference in conjunction with GlobeCom'94, Nov. 1994, San Francisco. This research was carried out in part at the Jet Propulsion Laboratory, California Institute of Technology, under a contract with NASA

1 Introduction

Continuous Phase Modulation (CPM) is a class of constant envelope modulation schemes. CPM can have power and bandwidth efficiency, so it is an attractive scheme to be used whenever a nonlinear channel is employed (requires constant amplitude signal). With the addition of an encoder in front of the modulator, even better combinations of power and bandwidth efficiency are possible. However, to enjoy these benefits, optimum coherent detection of CPM frequently requires complex receivers and difficult carrier tracking. Due to the difficulty in achieving coherency in CPM systems, many noncoherent receivers were suggested in the literature. Here, we propose a new method for combined noncoherent detection and decoding of CPM which can be also used for coded CPM.

Data detection and carrier phase tracking, as two separate problems, have been studied extensively in the past. Uncoded or coded CPM over the Additive White Gaussian Noise (AWGN) channel with coherent detection can be optimally decoded by the Viterbi Algorithm (VA) [2]. The carrier phase tracking can be performed by a Phase Locked Loop (PLL). There are two ways to implement the phase tracking for CPM. One is to remove the data by a nonlinear operation, and then lock to one or more of the discrete spectral components produced [2]. The other is to decode the data and feed it back into the loop (data aided loop) [3]. If discrete spectral components are to be generated from a CPM scheme with R phase states, the signal has to be raised to the Rth power. Since this process results in a large SNR (Signal to Noise Ratio) drop, very narrow loops must be employed. For the data aided loop, the large decoding delay caused by the VA will only allow the operation of a PLL with a large time constant (narrow-band). Some improvement can be potentially gained by using premature decisions from the VA to reduce the delay [4]. Data aided based PLL also have the danger that few erroneous decisions can cause loss of lock. A narrow band PLL is usually required, but such a PLL cannot be used for the cases where fast phase variations in the channel occur due to phase noise or Doppler effects. PLL's in general cause problems like slow and difficult acquisition, and delayed recognition of loss of lock, slow recovery from fade, and false lock.

In many cases, noncoherent methods are more preferred than PLL's since they are more

resistant to fading, they allow burst operation, and they stand higher phase noise. Differential And Limiter-Discriminator (LD) detectors in their basic forms, have a minimum degradation of about 3 dB on AWGN relative to coherent detection, and this is only for certain binary CPM schemes. For other, more powerful schemes, the degradation is even higher. Many methods were used to improve the performance of these detectors including zero forcing equalizer, decision feedback, error correction and VA. A good comparison is found in [23] for the case of MSK (Minimum Shift Keying). The best of these schemes provides 2 dB degradation for MSK with LD and decision feedback.

It is useful to compare between noncoherent schemes on the basis of the observation length L in symbols. The observation length is the length the channel phase can be assumed constant, and is inversely related to the resistance of the scheme to phase jitter. In addition, in many schemes the complexity is exponential in L. Makrakis [17] has shown degradation of 1.5 dB for Gaussian Minimum Shift Keying (GMSK) with $BT_s = 0.25$ (B is the 3db Bandwidth of the shaping filter and T_s is the bit duration), by combining 3 differential detectors for delays of 1,2 and 3 symbols and using VA. Note that the lower degradation mentioned in [17] is due to comparison to sub-optimal coherent detection of [26] instead of to the optimal. The observation length is equivalent to 4 symbols. Note that their scheme requires the addition of a differential encoder in front of GMSK. This alone causes unrecoverable degradation of 0.5 dB even if the number of differential detectors is increased to infinity. It will be interesting to know the performance of Makrakis et al. method for other CPM schemes, including multilevel ones.

Obsborne and Luntz [19], and then Aulin et al. [20], [21] solves a noncoherent MLSE (Maximum Likelihood Sequence Estimator) decision on a block of L symbols, but decides only on one symbol. The complexity is exponential in L, but there exist a suboptimal version which uses the Viterbi algorithm. For most evaluated schemes, $L > 10$ is required to approach coherent performance. Simon et. al. [24], made an MLSE decision on all L symbols. Leib et. al. [23] and Abrardo et al. [25] have recognized that the symbols at the edge of the block have a higher contribution to the error probability and ignore them, getting improved results. In [23], the degradation of noncoherent detection of MSK is 1.4 dB for $L = 8$. In [25],

degradation of less than 0.5 dB is shown with $L = 7$ for GMSK, $BT = 0.5$. This compares to $L = 4$ in our scheme (see Figure 6). Harrold et. al. [22] have suggested another scheme, based on the VA algorithm where a phase estimation is made from the best survivor and used as a reference to evaluating a partially coherent metric on an observation. In their scheme, $L = 12$–25 is required to be close within 0.5 dB to coherent detection with various partial response schemes, but the complexity is not exponential in L. There is no data to compare to for noncoherent decoding of coded CPM.

Our scheme outperforms all of the above noncoherent schemes in terms of the required observation for achieving close to coherent performance. $L = 3$ only is required for MSK, and $L = 5$–6 for good 4 level schemes including partial response. For GMSK, $BT = 0.25$, in particular, [17] shows similar performance, but the results for additional CPM types should be provided for comparison. Note that reduced complexity algorithms are not available for this method.

We apply noncoherent decoding also to coded CPM. Anderson at el. [7] considered convolutionally coded CPM. However, they used the unrealistic assumption that the phase is constant forever. Their method can be used if for each symbol decision a large block is processed, large enough to contain the longest probable error event. This block becomes larger as the SNR drops. A large block means a very large observation and prohibitive complexity. Poor results are expected when applying differential detection or LD to coded CPM since the working point is at low symbol SNR. The previously proposed MLSE methods cannot be applied to coded CPM, unless the observations do not overlap. In this case worse performance is expected as was demonstrated for uncoded CPM, and for coded BPSK (Bipolar Phase Shift Keying) [1].

Unlike the previous schemes using multiple-symbol observations, the method described in this paper uses fully overlapped observations, such that the observations are not independent. In this way the channel phase memory is used in a much more efficient way. This method was first used for multiple-symbol overlapped observations of trellis coded PSK modulation [1]. Here we apply the technique to CPM. Since CPM has a trellis structure, many of the concepts in [1] and [5] can be applied to CPM. In addition, the sub-optimal algorithms of [5]

have remarkably low degradation when applied on CPM.

Noncoherently catastrophic (NC)[1] codes are those where there exists at least two sequences which differ in a constant phase shift, and are the encoding of different input. CPM is clearly not NC. Although many sequences which are a constant phase shift of another exist, all of these are the encoding of the same input symbols. Coded CPM is not NC, since the encoder only generates a subset of the uncoded CPM outputs, and uncoded CPM is not NC. Hence, unless the encoder itself is catastrophic, the coded CPM will not be NC.

2 CPM Schemes

In CPM schemes, the envelope of the RF (Radio Frequency) signal is constant and its phase varies in a continuous manner. CPM signals are described by

$$s_n(t) = \frac{1}{\sqrt{T_s}} \exp\left\{ j2\pi \sum_{i=0}^{n} h a_i q(t - iT_s) \right\} \quad \text{for} \quad nT_s < t < (n+1)T_s. \tag{1}$$

The data $\{a_n\}$ are M-ary data symbols of duration T_s, M is usually a power of 2, taken from the alphabet $\pm 1, \pm 3 \cdots, \pm(M-1)$, h is a modulation index and $q(t)$ is the phase response function. CPM schemes are denoted by their phase response function or by its derivative $g(t)$, the frequency response function. Let G be the number of symbol intervals over which the frequency response function is not zero. The phase response satisfies $q(t) = 0$ for $t < 0$ and $q(t) = 1/2$ for $t > GT_s$. If $G = 1$, the scheme is called full response, and when $G > 1$ it is called partial response. The full response CPM with rectangular frequency pulse is called CPFSK (Continuous Phase Frequency Shift Keying). Binary CPFSK with $h = 1/2$ is called MSK (Minimum Shift Keying).

3 The Noncoherent Sequence Estimation

The derivation of the optimal Noncoherent Maximum Likelihood Sequence Estimator (NMLSE) depends on the statistics of the time varying carrier phase. When such statistics are unavailable, the derivation of the optimal NMLSE must start from some broad assumptions. The commonly used assumption is that the carrier phase is constant (but completely unknown) during some observation interval $(t, t+T)$.

In the previous approaches, the observations were used independently. We use maximally overlapped observations which make use of the fact that the carrier phase can be assumed to be constant for *any* observation of length T. This uses the channel memory in a more efficient way. However, for the derivation of the estimator itself, we assume that the observations, even when they overlap in time, are independent, and have independent phases. We call the resulting sub-optimal estimator Independent Overlapped observations NMLSE (IO-NMLSE). Note that the observations are not made independent by any mean, they are only treated as such for the derivation of the estimator. During this paper x^* means complex conjugation and $\mathbf{A}^\dagger$ means conjugate and transpose of the matrix $\mathbf{A}$.

The IO-NMLSE discriminates between a set of possible transmitted waveforms $\{x_i(t)\}$ with constant energy symbols by choosing m which maximizes the following metric

$$\eta(x^{(m)}(t)) = \sum_{k=-\infty}^{\infty} \left| \int_{k\tau-T}^{k\tau} r(t)^* x^{(m)}(t) dt \right|^2, \tag{2}$$

where $r(t)$ is the received waveform (both $x(t)$ and $r(t)$ are complex baseband signal), k is the observation number, τ is the observations spacing (chosen as small as possible) and T is the observation length. In the digital implementation, $x^{(m)}(t)$ is a sequence of symbols of duration T_s, each denoted by $x_n^{(m)}(t)$. Let the vector $\bar{\mathbf{x}}_n^{(m)}$ of dimension D be the signal space representation of $x_n^{(m)}(t)$. Then the metric can be written as

$$\eta(\bar{\mathbf{x}}^{(m)}) = \sum_{k=-\infty}^{\infty} \eta_k = \sum_{k=-\infty}^{\infty} \left| \sum_{i=0}^{L-1} \bar{\mathbf{r}}_{lk-i}^\dagger \bar{\mathbf{x}}_{lk-i}^{(m)} \right|^2, \tag{3}$$

where L is the observation length in symbols ($T = LT_s$), l is the observations spacing in symbols ($\tau = lT_s$) and for every symbol interval n, $\bar{\mathbf{r}}_n$ is a complex vector which assumes the output of D complex matched filters, each for one complex dimension of modulation. In this paper we assume $l = 1$ (maximal overlap). For CPM, we can choose an orthonormal basis such that D is finite. In practice we can use the Gram-Schmidt orthogonalization procedure for finding the basis functions (for the simulation program). In general, $D \leq M^G$.

For any code which is not noncoherently catastrophic, as L increases (and the allowed phase variations are reduced appropriately), the performance of the IO-NMLSE approaches

that of the MLSE with a completely known phase [1]. This provides a tradeoff between robustness to phase variations and power efficiency.

4 A Trellis Structure for Use in Noncoherent CPM

A CPM scheme with a rational modulation index h can be represented by a trellis diagram. In a full response scheme, the states are the phase states, and in a partial response scheme, a state corresponds to the phase state and $G-1$ last symbols [2]. We can use this trellis as a basis to decoder implementation. However, specifically for CPM, we can make some simplifications to reduce the number of states and to improve the understanding of the factors influencing the performance of the noncoherent system.

We like to use the VA to implement the IO-NMLSE. When we use the VA to maximize (3), we use η_k as branch metric. The symbols indexed by $k-i$, $i=1,\ldots,L-1$, are taken from the survivor path, i.e., decision feedback is involved. This modification of the VA is called Basic Decision Feedback Algorithm (BDFA) [5]. This algorithm is of similar principle as the Reduced States Sequence Estimator (RSSE) [32] used for ISI channels and belongs to the class of decoders called per survivor processing [33].

The BDFA, applied on the original trellis of a code, is suboptimal. We have to construct a new trellis diagram to apply the BDFA which will be called an "optimal trellis". Using this trellis in the BDFA results in optimal operation,i.e., the metric (3) is maximized.

Moreover, the phase states carry unuseful information for the noncoherent decoder, so they can be eliminated.

Let us begin by defining a new trellis diagram for CPM in which the phase states are eliminated, but otherwise all the waveforms can be generated without any change. We will call this trellis the *primitive noncoherent trellis*. The primitive trellis is the optimal one for the case of $L=1$, i.e., symbol by symbol noncoherent detection. Each state in the primitive noncoherent trellis corresponds to the last $G-1$ input symbols $\{a_{n-1}, a_{n-2}, \cdots, a_{n-G+1}\}$. The $G-1$ symbols correspond to the memory required by the partial response scheme. Note that for a full response scheme, the trellis has only one state and M parallel transitions. Let $s_n(t)$

be the output waveform for the duration of the symbol a_n,

$$s_n(t) = \frac{1}{\sqrt{T_s}} \exp\Big\{ j2\pi h \sum_{i=-\infty}^{n} a_i q(t - iT_s) \Big\} =$$

$$= \frac{1}{\sqrt{T_s}} \exp\Big\{ j2\pi h \sum_{i=0}^{G-1} a_{n-i} q(t - iT_s) + jh\pi \sum_{i=-\infty}^{n-G} a_i \Big\},$$

$$nT_s \leq t \leq (n+1)T_s, \tag{4}$$

and let $s'_n(t)$ be the same waveform as $s_n(t)$ but with a zero phase state,

$$s'_n(t) = \frac{1}{\sqrt{T_s}} \exp\Big\{ j2\pi h \sum_{i=0}^{G-1} a_{n-i} q(t - iT_s) \Big\}. \tag{5}$$

Each branch of the trellis is assigned a record with two information fields. The first field contains $s'_n(t)$, and the second field contains the amount of phase rotation induced by the input symbol a_{n-G+1},

$$\theta_n = \pi h a_{n-G+1}. \tag{6}$$

Given a sequence $\{s'_n(t), \theta_n\}$, starting at time n_0 (which may be the beginning of an observation), the signal $s_n(t)$ can be derived, up to a constant phase shift ϕ as

$$s_n(t) = s'_n(t) \exp\Big\{ j \sum_{i=n_0}^{n-1} \theta_i + j\phi \Big\}. \tag{7}$$

An example of the primitive noncoherent trellis is shown in Figure 1-b for the case of CPFSK with $h = 2/5$ and $M = 2$. For reference the coherent trellis where the phase state are present is shown in Figure 1-a. The optimal noncoherent trellis for $L > 1$ must allow for the additional memory introduced by the overlapping. Each state in the optimal noncoherent trellis corresponds to the last $L - 1 + G - 1$ input symbols $\{a_{n-1}, a_{n-2}, \cdots, a_{n-L-G+2}\}$. The $L-1$ symbols correspond to the amount of overlapping between the observations which can be considered as the amount of memory, and $G - 1$ symbols correspond to the memory required by the partial response. The assignments of the branches, as in the primitive trellis, follow equations (5) and (6). If a shift register is used as an encoder, then the most recent $G - 1$ symbols, together with the current input, are used to choose one of the possible M^G waveforms (or complex vectors representing these waveforms). The rest of the shift register stages are

left unconnected. These stages are only used for the purpose of delaying the merge of two sequences on the trellis by $L-1$ symbols, see an example in Figure 1-c and Figure 1-d. During this "waiting period" the outputs of the two sequences are equal. Now the future symbols after the merge have no influence on the result of the comparison between the candidates' paths, so tentative decisions can be made, enabling the optimal use of the VA.

5 Computing the Error Probability of the IO-NMLSE for CPM Signals

In CPM, the error probability is not independent of the transmitted sequence. There is a way to overcome this problem, by using a trellis diagram that represents the phase difference between two CPM signals. The error probability of a constant energy coded modulation can be completely specified by the pairwise complex correlations of all possible waveforms (which here is equivalent to the phase difference). This is known for the coherent detection case. In [8] it was proved that it is also true for any arbitrary maximum-likelihood type detector which uses a correlator front end.

Since there is a linear mapping from input symbols to output phases, the phase difference signal can be generated simply by feeding the difference of the input symbols through the CPM transmitter. Also, we can form a different trellis diagram which is similar to the previously defined trellis, but where the input symbols a_n are replaced by difference input symbols Δa_n. Each symbol a_n takes the values $\pm 1, \pm 3, \cdots, \pm(M-1)$, and Δa_n takes the values $0, \pm 2, \pm 4, \cdots, \pm 2(M-1)$, i.e., $2M-1$ values. Refer to Figure 1-e and 1-f for an example.

Let the channel be AWGN with slowly varying carrier phase. For error probability computation, we assume that a specific codeword is transmitted, namely the all-0 difference sequence, and find the probability that another path on the trellis attains a larger metric.

The value of the metric (3) is independent of the carrier phase process as long as the assumption of constant phase over L symbols approximately holds. Thus, we can assume without loss of generality that the phase is constant everywhere and is equal to zero. This analysis holds for any arbitrary slowly varying phase process.

Unfortunately, the pairwise error probability can not be expressed in a form suitable for

the transfer function method. Instead, we numerically compute the truncated union bound and approximate the bit error probability as (see [2])

$$P_b \cong \frac{1}{\log_2 M} \sum_{|\bar{\mathbf{x}}^{(m)}|<K} b(\bar{\mathbf{x}}^{(m)}) P_e\{\bar{\mathbf{x}}^{(m)}\} \prod_{n=0}^{N-1} \frac{M - |\Delta a_n|/2}{M} \tag{8}$$

where $\bar{\mathbf{x}}^{(m)}$ are all possible competing sequences, $|\bar{\mathbf{x}}^{(m)}|$ is the length of the error event, $b(\bar{\mathbf{x}}^{(m)})$ is the hamming weight of the error and K is a sufficiently large number such that the residual contribution of the larger error events can be neglected. $P_e\{\bar{\mathbf{x}}^{(m)}\}$ is the pairwise error probability between the all-0 sequence and $\bar{\mathbf{x}}^{(m)}$. The last term in the expression corresponds to the fact that every difference sequence may represent more than one pair of input sequences [2].

Let us position the beginning of the error event at $L-1$, and its ending point will be denoted by $N-1$. The computation of the pairwise error probability used in [1] involves matrixes with size DN. For CPM, with partial response, D is large, so the method becomes computationally too extensive. Here we develop a method which uses only the values of the correlations between symbols and thus is independent of D. The size of the matrixes involved will be always $2N$. We know that such derivation is possible using the results in [8].

Let $\bar{\mathbf{x}}_n$ be one of the sequences $\bar{\mathbf{x}}^{(m)}$ and $x(t)$ be its corresponding continuous waveform. Note that $\bar{\mathbf{x}}_n$ has unit energy. Let us assume that $\bar{\mathbf{r}}_n$ is normalized such that $\bar{\mathbf{r}}_n = \sqrt{E_s}\bar{\mathbf{x}}_n + \bar{\mathbf{n}}_n$, where $E_s = (2\log_2 M E_b)/N_0$, E_b is the energy per bit, N_0 is the noise spectral density and $\bar{\mathbf{n}}_n$ are independent complex vectors of independent normal components with unit variance and zero mean.

Let $\alpha_n = \bar{\mathbf{x}}_n^\dagger \bar{\mathbf{r}}_n = \int_{nT_s}^{(n+1)T_s} r(t)x^*(t)dt$ and $\beta_n = \mathcal{Z}^\dagger \bar{\mathbf{r}}_n = \int_{nT_s}^{(n+1)T_s} r(t)dt$, where $\mathcal{Z}$ is the d.c. symbol ($s_n(t) = 1/\sqrt{T_s}$ in the orthonormal basis). Let

$$Y_1 = \sum_{k=L-1}^{N-1} \left| \sum_{i=0}^{L-1} \beta_{k-i} \right|^2 \tag{9}$$

and

$$Y_2 = \sum_{k=L-1}^{N-1} \left| \sum_{i=0}^{L-1} \alpha_{k-i} \right|^2. \tag{10}$$

Then $P_e\{\bar{\mathbf{x}}\} = \Pr\{Y_2 > Y_1\}$.

$$Y_2 = \sum_{k=L-1}^{N-1} (\sum_{i=0}^{L-1} \alpha_{k-i})^* (\sum_{j=0}^{L-1} \alpha_{k-j}) = \sum_{k=L-1}^{N-1} \sum_{i=0}^{L-1} \sum_{j=0}^{L-1} \alpha^*_{k-i}\alpha_{k-j} = \tag{11}$$

$$= \sum_{k=0}^{N-L} \sum_{p=k}^{k+L-1} \sum_{q=k}^{k+L-1} \alpha^*_p \alpha_q = \sum_{p=0}^{N-1} \sum_{q=0}^{N-1} \alpha^*_p \alpha_q \sum_{k=0}^{N-L} w(p,q,k), \tag{12}$$

where

$$w(p,q,k) = \begin{cases} 1, & \text{if } k \le p,q \le k+L-1; \\ 0, & \text{otherwise} \end{cases}. \tag{13}$$

Let

$$a_{p,q} = \sum_{k=0}^{N-L} w(p,q,k) \tag{14}$$

and let $\mathbf{A} = \{a_{p,q}\}$, a $N \times N$ matrix, then

$$Y_2 = \underline{\alpha}^\dagger \mathbf{A} \underline{\alpha} \quad \text{and,} \quad Y_1 = \underline{\beta}^\dagger \mathbf{A} \underline{\beta}, \tag{15}$$

where $\underline{\alpha}$ and $\underline{\beta}$ are vectors with components α_p and β_p, $0 \le p \le N-1$. Let

$$Y = Y_2 - Y_1 = \underline{\alpha}^\dagger \mathbf{A} \underline{\alpha} - \underline{\beta}^\dagger \mathbf{A} \underline{\beta}. \tag{16}$$

Let us define the vector $\underline{u}$ of length $2N$ as

$$\underline{u} = \begin{pmatrix} \underline{\alpha} \\ \underline{\beta} \end{pmatrix}, \tag{17}$$

and the $2N \times 2N$ matrix $\mathbf{P}$ as

$$\mathbf{P} = \begin{pmatrix} \mathbf{A} & 0 \\ 0 & -\mathbf{A} \end{pmatrix}. \tag{18}$$

Then,

$$Y = \underline{u}^\dagger \mathbf{P} \underline{u}. \tag{19}$$

Let $\mathbf{V}$ be the covariance matrix of $\underline{u}$. Its nonzero entries are

$$v_{p,p} = E\{[\alpha_p - E(\alpha_p)][\alpha^*_p - E(\alpha_p)^*]\} = \tag{20}$$

$$= E\{\bar{\mathbf{x}}^\dagger_p [\bar{\mathbf{r}}_p - E(\bar{\mathbf{r}}_p)][\bar{\mathbf{r}}_p - E(\bar{\mathbf{r}}_p)]^\dagger \bar{\mathbf{x}}_p\} = \bar{\mathbf{x}}^\dagger_p \mathbf{I} \bar{\mathbf{x}}_p = \bar{\mathbf{x}}^\dagger_p \bar{\mathbf{x}}_p = 1,$$

where $\mathbf{I}$ is the identity matrix,

$$v_{p,p+N} = E\{[\alpha_p - E(\alpha_p)][\beta^*_p - E(\beta_p)^*]\} = \tag{21}$$

$$E\{\bar{\mathbf{x}}_p^\dagger[\bar{\mathbf{r}}_p - E(\bar{\mathbf{r}}_p)][\bar{\mathbf{r}}_p - E(\bar{\mathbf{r}}_p)]^\dagger \mathcal{Z}\} = \bar{\mathbf{x}}_p^\dagger \mathcal{Z} = \frac{1}{T_s}\int_{pT_s}^{(p+1)T_s} x_p(t)dt \triangleq u_p,$$

and

$$v_{p+N,p} = v_{p,p+N}^*. \tag{22}$$

$$\mathbf{V} = \begin{pmatrix} 1 & & & & u_0 & & & \\ & 1 & & & & u_1 & 0 & \\ & & \ddots & & 0 & & \ddots & \\ & & & \ddots & & & & u_{N-1} \\ u_0^* & & 0 & & \ddots & & & \\ & u_1^* & & & & \ddots & & \\ & 0 & \ddots & & & & \ddots & \\ & & & u_{N-1}^* & & & & 1 \end{pmatrix}. \tag{23}$$

Here we have a non-central indefinite quadratic form in normal random variables, where the random variables are also correlated. There is a well known method for diagonalization of such a quadratic form [27] summarized as follows. Let us find a non-singular matrix $\mathbf{L}$ such that $\mathbf{V} = \mathbf{L}^\dagger\mathbf{L}$. Since $\mathbf{V}$ is Hermitian, such decomposition always exists [28] and is not unique. Let us define another random vector related to $\underline{u}$ as

$$\underline{w} = \mathbf{L}^{-1^\dagger}\underline{u}. \tag{24}$$

The following relations are useful to note: $\mathbf{L}^{-1^\dagger} = \mathbf{L}^{\dagger^{-1}}$ and $(\mathbf{L}^\dagger\mathbf{L})^{-1} = \mathbf{L}^{-1}\mathbf{L}^{-1^\dagger}$. The covariance matrix of $\underline{w}$ is

$$E\{[\underline{w} - E(\underline{w})][\underline{w} - E(\underline{w})]^\dagger\} = \mathbf{L}^{-1^\dagger}E\{[\underline{u} - E(\underline{u})][\underline{u} - E(\underline{u})]^\dagger\}\mathbf{L}^{-1} =$$

$$= \mathbf{L}^{-1^\dagger}\mathbf{V}\mathbf{L}^{-1} = \mathbf{L}^{-1^\dagger}\mathbf{L}^\dagger\mathbf{L}\mathbf{L}^{-1} = I. \tag{25}$$

Hence, the components of $\underline{w}$ are uncorrelated. Let us use (24) in (19) to get

$$Y = \underline{w}^\dagger\mathbf{L}\mathbf{P}\mathbf{L}^\dagger\underline{w}. \tag{26}$$

Let Λ be the diagonal eigenvalue matrix of $\mathbf{L}\mathbf{P}\mathbf{L}^\dagger$ and $\mathbf{Q}$ the unitary eigenvector matrix. If we set $\underline{z} = \mathbf{Q}^\dagger\underline{w}$, then

$$Y = \underline{w}^\dagger\mathbf{Q}\Lambda\mathbf{Q}^\dagger\underline{w} = \underline{z}^\dagger\Lambda\underline{z} = \sum_{i=0}^{2N-1}\lambda_i|z_i|^2. \tag{27}$$

The Gaussian random vector $\underline{z}$ is composed of uncorrelated components with unit variance and mean

$$E[\underline{z}] = \mathbf{Q}^{\dagger}\mathbf{L}^{-1\dagger}E[\underline{u}], \tag{28}$$

where

$$E[\underline{u}] = \sqrt{E_s}\begin{pmatrix} 1 \\ 1 \\ \vdots \\ 1 \\ u_0 \\ u_1 \\ \vdots \\ u_{N-1} \end{pmatrix}. \tag{29}$$

Finally,

$$P_e\{\mathbf{x}\} = \Pr\{Y > 0\} = \Pr\Big\{\sum_{i=0}^{2N-1} \lambda_i |z_i|^2 > 0\Big\}. \tag{30}$$

The pairwise error probability computation requires the evaluation of the distribution of the indefinite and non-central Hermitian form in normal random variables (30). Its characteristic function is known and can be found in [27] (note that here the random variables are complex):

$$\Phi(\omega) = \exp\Big\{-\frac{1}{2}\sum_{i=0}^{2N-1}|\mu_i|^2 + \frac{1}{2}\sum_{i=0}^{2N-1}\frac{|\mu_i|^2}{1-2\lambda_i j\omega}\Big\}\prod_{i=0}^{2N-1}\frac{1}{1-2\lambda_i j\omega}, \tag{31}$$

where $\mu_i = E[z_i]$. This characteristic function should be inverted in order to find the distribution of Y. The distribution was computed by a numerical method [1, App. B] since there is no closed form expression, neither a convenient series expression.

The matrix $\mathbf{L}$ can be found by standard triangular factorization techniques. However, for our particular case we were able to find a closed form for $\mathbf{L}$ (one of many possible solutions). The validity of the following expressions can be confirmed by inspection.

$$\mathbf{L} = \begin{pmatrix} u_0^* & 0 & \dots & \dots & 1 & 0 & \dots & 0 \\ \sqrt{1-|u_0|^2} & 0 & \dots & \dots & 0 & 0 & \dots & 0 \\ 0 & u_1^* & \dots & \dots & 0 & 1 & \dots & 0 \\ 0 & \sqrt{1-|u_1|^2} & \dots & \dots & 0 & 0 & \dots & 0 \\ \vdots & \vdots & \ddots & & \vdots & \vdots & \ddots & \vdots \\ 0 & 0 & \dots & u_{N-1}^* & 0 & 0 & \dots & 1 \\ 0 & 0 & \dots & \sqrt{1-|u_{N-1}|^2} & 0 & 0 & \dots & 0 \end{pmatrix}, \tag{32}$$

and

$$\mathbf{L}^{-1} = \begin{pmatrix} 0 & \frac{1}{\sqrt{1-|u_0|^2}} & 0 & 0 & \dots & \dots & 0 \\ 0 & 0 & 0 & \frac{1}{\sqrt{1-|u_1|^2}} & \dots & \dots & 0 \\ \vdots & \vdots & \vdots & & & \ddots & \vdots \\ 0 & 0 & 0 & 0 & \dots & 0 & \frac{1}{\sqrt{1-|u_{N-1}|^2}} \\ 1 & -\frac{u_0^*}{\sqrt{1-|u_0|^2}} & 0 & 0 & \dots & 0 & 0 \\ 0 & 0 & 1 & -\frac{u_1^*}{\sqrt{1-|u_1|^2}} & \dots & 0 & 0 \\ \vdots & \vdots & & & & \vdots & \vdots \\ 0 & 0 & 0 & 0 & \dots & 1 & -\frac{u_{N-1}^*}{\sqrt{1-|u_{N-1}|^2}} \end{pmatrix}. \tag{33}$$

6 Performance Predictions

The degradation of the noncoherent methods versus the coherent ones comes from two sources. One is the increase in the error probability for error events which also occur in the coherent case and the other source is due to the inclusion of additional error events, which cannot occur in coherent reception. The additional error events are those which start in the transmitted sequence and diverge to a sequence with a constant phase shift from the transmitted one. In a noncoherent CPM trellis diagram, these error events can be distinguished by having a total phase rotation, $\sum \theta_n$, different from that of the transmitted sequence. In a coherent CPM trellis, this will correspond to reaching a different phase state, so that there would not be a merge, and thus no error event. The contribution of the additional error events is lower as the observation length, L, grows. In particular, when L is larger than the error event length, there are some observations that span the region of before and after the error event. These observations will have a particularly large distance and thus low error probability. Error events with larger difference in the total phase rotation tend to have lower pairwise error probability for the same event length.

For this reason CPM schemes which use h near a "weak" point will suffer a larger degradation (only if this weak point causes poor performance). A weak modulation index, [2] means that a merge can happen prior to the first inevitable merge at $t = (G+1)T_s$. Suppose that a weak modulation index h_w, causes a reduction in the minimum distance. Let $\mathbf{a}$ and $\mathbf{b}$ be two

sequences of input symbols which correspond to two paths on the coherent trellis which start at state 0 at time $t = 0$ and merges at time $t = t_0 \leq GT$, for $h = h_w$. Now, if we use for the same CPM scheme h close to h_w, then at time t_0 the two sequences **a** and **b** will reach two different phase states ϕ_a and ϕ_b. It is clear that for $h \sim h_w$, $\phi_a - \phi_b \cong 0$. On the primitive noncoherent trellis, **a** and **b** correspond to two paths that merge at t_0 or prior to that. At t_0 the total phase rotations of **a** and **b** are equal to ϕ_a and ϕ_b respectively. Thus, the difference in the total phase transition for this error event is small, possibly having a large probability to occur in the noncoherent decoder.

In order to get some rough approximation on the required observation length for different modulation schemes, we introduce the following arguments. Suppose that a constant phase is transmitted, $x_0(t) = 1$ (usually corresponding to the all-0 input to a code or modulator). Let us have another candidate sequence, $x_1(t)$. Note that by letting $x_0(t)$ and $x_1(t)$ be phase difference sequences, the following discussion applies to any transmitted sequence. The operation

$$\left| \int_{k\tau}^{k\tau+T} r(t)x^*(t)dt \right|^2$$

is equivalent to the signal passed through a filter with an impulse response $h(t) = x^*(T - t)$ and taking the squared magnitude of the result, sampled at time $t = T$. The operation of equation (2) is to consider all possible sampling points, with some finite resolution τ. The impulse response in the case of the candidate $x_0(t)$ is

$$h(t) = 1, \quad 0 \leq t \leq T.$$

This corresponds to a low-pass filter. In order to have the largest distance between $x_0(t)$ and $x_1(t)$ in one observation (here distance serves as a qualitative term only), $x_1(t)$ has to contain most of its energy in high frequency. Then for this observation the calculation of the metric of $x_1(t)$ will be equivalent to the energy output of a high pass filter. Passing $x_0(t)$, a low pass signal through this filter will result in a low output. Hence to get low error probability performance using the shortest observations, the energy of $x_1(t)$ should be concentrated at as high frequency as possible, see Example 6.1. Note that as the observation length T decreases, the equivalent low pass filter of the observations of $x_0(t)$ broadens and the same happens to the high pass properties of $x_1(t)$.

Instead of using the concept of filtering, we can consider the correlation between the signals over an observation. For a one observation noncoherent decision, the correlation determines the error probability. Both views are mathematically equivalent.

The high pass property of the events is indirectly related to the bandwidth occupancy and the spectral properties of the scheme as a whole. As the scheme becomes more bandwidth efficient, larger observations (measured in input bits) are required to achieve good error performance. This is true for the coded PSK schemes and also for the CPM (Continuous Phase Modulation) schemes. Take for example GMSK (Gaussian Minimum Shift Keying) [26]. GMSK with parameter $BT = \infty$ is equal to MSK (Minimum shift keying). GMSK improves its spectral properties as BT decreases. With $BT = 0.25$ it has much lower sidelobes than MSK. Correspondingly, GMSK with parameter $BT = 0.25$ requires $L = 10$ to be 0.5 dB close to coherent. With $BT = 0.5$, $L = 4$ is required, whereas in MSK only $L = 3$ is required (see Figures 5–8).

Additional arguments why bandwidth efficient schemes requires longer observations are found in [1] and [2].

Example 6.1 *Let us have a code with the following three codewords (in one complex dimension), transmitted over the AWGN channel:*

$$\mathbf{x}^{(0)} = \{\ldots, 1, 1, 1, 1, \ldots\},$$

$$\mathbf{x}^{(1)} = \{\ldots, 1, 1, j, j, 1, 1, \ldots\},$$

and

$$\mathbf{x}^{(2)} = \{\ldots, 1, 1, j, -j, 1, 1, \ldots\}.$$

Let $\mathbf{x}^{(0)}$ *be the transmitted codeword.* $\mathbf{x}^{(2)}$ *has more high energy content than* $\mathbf{x}^{(1)}$. *Both* $\mathbf{x}^{(1)}$ *and* $\mathbf{x}^{(2)}$ *have the same probability to be detected instead of the true message when coherent decoding is used. However, when noncoherent decoding is used, we have found that for* $\mathbf{x}^{(1)}$ *we need* $L = 7$ *for getting close (within* 0.5 *dB) to coherent error probability but for* $\mathbf{x}^{(2)}$ *we need only* $L = 2$*!*

7 Coded CPM

It is possible to encode the input data prior to feeding it to the CPM modulator and achieve a significant coding gain. Some good convolutional encoders for CPM (coherent detection) were found using a systematic search [9]-[11].

Evaluating the performance of binary encoded CPM is more difficult than uncoded CPM since it is not possible to use the symbol-difference trellis and assume the all-0 sequence is transmitted. The encoder is implemented over GF(2) and not over the real field as the input symbols of the CPM modulator. It may be the subject of future research to find an equivalent method to the symbol-difference trellis for coded CPM. Evaluating the error probability for coded CPM can be done by using encoder-decoder pair-states trellis (see for example [30]) in conjunction with the analysis of Section 5.

We observed previously for the coded PSK case, that different codes, which have the same coherent performance, suffer different amounts of degradation in noncoherent decoding. Since we have not performed a systematic search for the best code for noncoherent CPM, we have to rely on good codes for the coherent decoding and hope that their degradation in noncoherent decoding is small even for a short observation. Of course we can always get close to the coherent performance if a large observation is used, and for this case the codes best for coherent decoding will be the best for noncoherent. Specifically, the code which we evaluate here suffers low degradation, hence probably it is close or equal to the best noncoherent code. The encoder for this code is shown in Figure 2, and its equivalent for simulation is shown in Figure 3, and the equivalent encoder for noncoherent decoding, $L = 3$ (for example), is shown in Figure 4.

8 The Application of Suboptimal Decoding Algorithms to CPM

The algorithms described in [5] are applicable to uncoded or coded CPM. The BDFA has been mentioned in Section 4. When applied on non-optimal trellis, there is an increase in the probability of error events and also error propagation. The Modified Decision Feedback Algorithm

is a similar algorithm, which tends to reduce the error propagation. The Estimated Future Decision Feedback Algorithm (EFDFA) is a more sophisticated algorithm with complexity 4–5 times larger than the BDFA and more memory requirements, but can get very close to optimal performance and is summarized briefly as follows. The algorithm uses a novel concept called "estimated future" to improve the decision process. A block of samples of the input signal is saved in memory. On this block two passes are made: backward process (BP) and forward process (FP). In the BP, MDFA is performed backwards, starting from the end of the block. The BP has to converge from the initial conditions at the end of the block, in which no particular state is used as a beginning state. After the backward process ends, we have the survivor paths belonging to each state at each time in the trellis within the block. These paths are used as estimated future paths, and are considered in the FP for better reliability in the decisions.

Some points are worth noting when attempting to apply these algorithms to CPM. All these algorithms can be applied on the primitive trellis. For CPFSK schemes, using only a one state trellis leads to poor performance. However, for any L, we have found that the performance was significantly improved when we used the trellis optimal for $L = 2$ (M states). For the partial response schemes (2RC and 3RC, i.e., raised cosine pulse shape spanning 2 or 3 symbols respectively, were tested), it is sufficient to use the primitive trellis to get good results. This means that for noncoherent decoding, the complexity for the 2RC scheme is about equal to that of CPFSK. In some cases, the number of states used in the suboptimal noncoherent decoder is lower than that of the coherent one due to the removal of the phase states.

For all the CPM schemes we have tested, the error propagation was minor and the backward convergence was extremely rapid (when a $L = 2$ trellis is used for CPFSK and primitive trellis is used for partial response). The error propagation is relatively low also for coded CPM. Thus, the EFDFA has negligible degradation when applied to CPM.

9 Results and Discussion

In this section we present analytic performance evaluation and simulation results for various examples. In the simulations we included a very simplified, but useful, model for the phase variations. In this model the phase noise is a first order Markov process with Gaussian transition probability distribution. This corresponds to frequency spectrum that behave as $1/f^2$. In practice this means that the phase variation between successive symbols is independent normal random variable, with zero mean and specified variance δ^2.

The first example is MSK modulation, see Figure 5. Analytic results are given, supplemented by simulation points for $L = 5$ ($\delta = 0, 5, 10°$/sym). The case $\delta = 0$ can be used to confirm the analysis. The EFDFA can be considered optimal in the CPM case, and the simpler algorithm BDFA's performance is also shown. The small difference between the simulation points and the analysis at low SNR is due to the use of the union bound technique in the analysis. The phase noise is "slowly varying" only in the mean. Fast changes happen occasionally and cause errors. These errors can be seen only in high SNR when the error probability due to thermal noise is small. This phenomena is not unique to our decoder; it will happen in any detection scheme.

In Figures 6 and 7, we show the performance of GMSK. With $BT = \infty$, GMSK becomes MSK. As BT becomes lower, the side-lobes become smaller, and also, to a lesser extent, the spectrum become narrower. We recognize by comparing Figure 5, 6 and 7 that as the spectral properties improve, the degradation in the noncoherent decoding is higher for the same observation length. The reason, as explained intuitively in Section 6, is that the high frequency components are important to the noncoherent decoder.

In Figure 8 we show the performance of a partial response scheme. Here we use 4-level 2RC with $h = 1/3$. This scheme is chosen to have the same power efficiency as MSK but have much better bandwidth efficiency (almost twice the throughput for 99% power bandwidth). In Figure 9 we use a 4-level CPFSK with $h = 2/5$. This scheme is chosen such that the bandwidth requirements are close to that of MSK, but the power efficiency is much better.

Comparing Figures 9 and 10, we can see that as the modulation index h approaches a weak point $h = 0.5$, the degradation of the noncoherent decoder increases, as expected. The

shorter observations, $L = 2$, $L = 3$, as expected, do not "feel" the effect of being near a weak h point (see Section 6). Note that although the degradation is higher, the performance of the $h = 4/9$ scheme is better than the $h = 2/5$ scheme. Since, unlike the coherent case, the number of phase states does not affect the decoder complexity, $h = 4/9$ should be chosen among the two.

A coded CPM scheme is evaluated by simulations only in Figure 11. The coherent points were simulated as well. They match with the results in [9] which were computed using union bound techniques. We see degradation of about 0.4 dB when $L = 10$ is used. Compared to the coded PSK schemes, considering the bandwidth efficiency which tend to increase to observation length needed, this is a good result.

The simulation points were produced using the EFDFA or the BDFA. For the simulation points shown in Figure 8, 4 states were used in the EFDFA, compared to $4^{10} = 1048576$ states required for the optimal algorithm! For the coded CPM, 8 states were used in the EFDFA. One extra unconnected stage was added to reduce the degradation of the MDFA. BDFA can be applied successfully to uncoded CPM as shown in the examples. However, when applied to coded CPM, large error propagation bursts degrade its bit error probability significantly. This limit its application to short observations only. The degradation of the BDFA does not vanish even when the number of states is raised to 32.

10 conclusion

We have shown that the noncoherent decoding technique of [1] and its suboptimal implementation algorithms [5] are very well suited for noncoherent decoding of CPM schemes. Using these algorithms we can use observation lengths of few symbols and achieve less than $0.5dB$ degradation relative to coherent performance with a relatively low complexity receiver. Not only the noncoherent decoder handles much higher values of phase noise, the acquisition, tracking, loop design and phase ambiguity resolving circuitry are saved and also degradation from imperfect phase estimation is eliminated.

References

[1] Raphaeli, "Noncoherent Coded Modulation," IEEE Transactions on Communications, vol. 44, no. 2, pp. 172–183, Feb. 1996.

[2] Anderson J. B., Aulin T., Sundberg C.E., *Digital Phase Modulation*. NY: Plenum, 1986.

[3] Mazur B.A., Taylor D.P., "Demodulation and Carrier Synchronization of Multi-h Phase Codes," IEEE Trans. Comm., Vol. 29, No. 3, pp. 257–266, Mar. 1981.

[4] M. Morelli, U. Mengali, G. Vietta, "Joint Phase and Timing Recovery With CPM Signals", IEEE Trans. on Comm., vol. 45, no. 7, pp. 867–875, July 1997.

[5] Raphaeli D., "Decoding Algorithms for the Noncoherent Coded Modulation," IEEE Transactions on Communication, vol. 44, no. 3, pp. 1–12, March 1996.

[6] Raphaeli D., Divsalar D.,"Noncoherent Detection of Continuous Phase Modulation using Overlapped Observations", IEEE Communication Theory Mini-Conference, GLOBECOM'94, San Francisco, pp. 191–195, Nov. 1994.

[7] Andersson S. T., Svensson N.B., "Noncoherent Detection of Convolutionally Encoded Continuous Phase Modulation," IEEE J. Sel. Comm., Vol. 7, No. 9, pp. 1402–1414, Dec. 1989.

[8] Raphaeli D., "Construction of Uniform Error Property Codes for Generalized Decoding", *IEEE Communication Theory Mini-Conference, GLOBECOM'95*, Singapore, pp. 12–16, Nov. 1995.

[9] Lindell G., Sundberg C.W., "An Upper Bound on the Bit Error Probability of Combined Convolutional Coding and Continuous Phase Modulation," IEEE Trans. Comm., Vol. 34, No. 5, pp. 1263–1269, Sep. 1988.

[10] Pizzi S.V., Wilson S.G., "Convolutional Coding Combined with Continuous Phase Modulation," IEEE Trans. Comm., Vol. COM-33, No. 1, pp. 20–29, Jan. 1985.

[11] Lindell G., Sundberg C.E., Aulin T., "Minimum Euclidean Distance for Combinations of Short Rate 1/2 Convolutional Codes and CPFSK Modulation," IEEE Trans. Comm., Vol. IT-30, No. 3, pp. 509–519, May 1984.

[12] Hirade K., Ishizuka M., Adachi F., Ohtani K., "Error-Rate Performance of Digital FM with Differential Detection in Mobile Radio Channels," IEEE Trans. Veh. Tech., VT-28, pp. 204–212, 1979.

[13] Simon M.K., Wang C.C., "Differential Versus Limiter-Discriminator Detection of Narrowband FM," IEEE trans. Comm., Vol. 31, No. 11, pp. 1227–1234, Nov. 1983.

[14] Aulin T., Sundberg C.E., "Detection Performance of band-Limited continuous Phase Modulation," GLOBECOM'82, Miami, FL, Conf. Rec., pp. E7.6.1–E7.6.7, Nov. 1982.

[15] Svensson A., Sundberg C.E., "On error Probability for Several Types of Noncoherent Detection of CPM," Globecom'84, Atlanta, GA, Conf. Rec., pp. 22.5.1–22.5.7, Nov. 1984.

[16] Makrakis D., Mathiopoulos P.T., "Differential Detection of Correlative Encoded Continuous Phase Modulation Schemes Using Decision Feedback," IEE Proceedings, Vol. 138, No. 5, pp. 473–480, Oct. 1991.

[17] Makrakis D., Feher K., "Multiple Differential Detection of Continuous Phase Modulation Signals," IEEE Trans. Comm., Vol. 42, No. 2, pp. 186–196, May 1993.

[18] Andrisano O., Chiani M., Verdone R., "Performance of Narrowband CPM Systems with Limiter-Discriminator-Integrator Detection and Decision Feedback Equalization in Mobile Radio Channels," IEEE Trans. Comm., Vol. 42, No. 2, pp. 166–176, May 1993.

[19] Obsborne W.P. , Luntz M.B., "Coherent and Non-coherent Detection of CPFSK," IEEE Trans. Comm., COM-22, no. 8, pp. 1023–1036, Aug. 1974.

[20] Aulin T., Sundberg C.E., "Partially Coherent Detection of Digital Full Response Continuous Phase Modulated Signals," IEEE Trans. Comm., Vol. COM-30, No. 5, pp. 1096–1117, May 1982.

[21] Svensson A., Aulin T., Sundberg C.E., "Symbol Error Probability Behavior for Continuous Phase Modulation with Partially Coherent Detection," AEU, Vol. 40, No. 1, pp. 37–45, 1986.

[22] Harrold W., Kingsbury N., "A Partially Coherent Detector for Continuous Phase Modulation," IEEE Selec. Comm., Vol. 7, No. 9, pp. 1415–1426, Dec. 1989.

[23] Leib H., Pasupathy S., "Noncoherent Block Demodulation of MSK with Inherent and Enhanced Encoding," IEEE Trans. Comm., Vol. 40, No. 9, pp. 1430–1441, Sep. 1992.

[24] Simon M.K., Divsalar D., "Maximum Likelihood Block Detection of Noncoherent Continuous Phase Modulation," IEEE Trans. Comm., Vol. 41, No. 1, pp. 90–98, Jan. 1993.

[25] Abrardo A., Benelli G., Cau G., "Multiple-Symbols Differential Detection of GMSK," Elect. Letters, Vol. 29, No. 25, pp. 2167–2168, Dec. 1993.

[26] Murota K., Hirade K., "GMSK Modulation for Digital Mobile Radio Telephone," IEEE Trans. Comm., Vol. 29, No. 7, pp. 1044-1050, July 1981.

[27] Johnson N. I., Kotz S., *Continuous Univariate Distributions-2.* NJ: John Wiley & Sons, 1970.

[28] Franklin J.N., *Matrix Theory*, New Jersey: Prentice-Hall, 1993.

[29] Viterbi A.J., Omura J.K., *Principles of Digital Communication and Coding.* McGraw-Hill, 1979.

[30] Muligan M.G., Wilson S.G., "An Improved Algorithm for evaluating trellis phase Codes," IEEE Trans. on Inf. Theory, Vol. IT-30, pp. 846–851, Nov. 1984.

[31] Raphaeli D., "Noncoherent Coded Modulation," California Institute of Technology, Ph.D. Thesis, 1994.

[32] Eyuboglu M. V. and Qureshi S. U. H. , "Reduced State Sequence Estimation with Set Partitioning and Decision Feedback", IEEE Trans. on Comm., pp 428–436, vol. 37, no. 5, May 1989.

[33] Raheli R., Polydoros A. Tzou C. K., "Per Survivor Processing: A General Approach to MLSE in Uncertain Environments", IEEE Trans. on Comm., vol. 43, No. 2/3/4, pp. 354–364, Feb/Mar/Apr 1995.

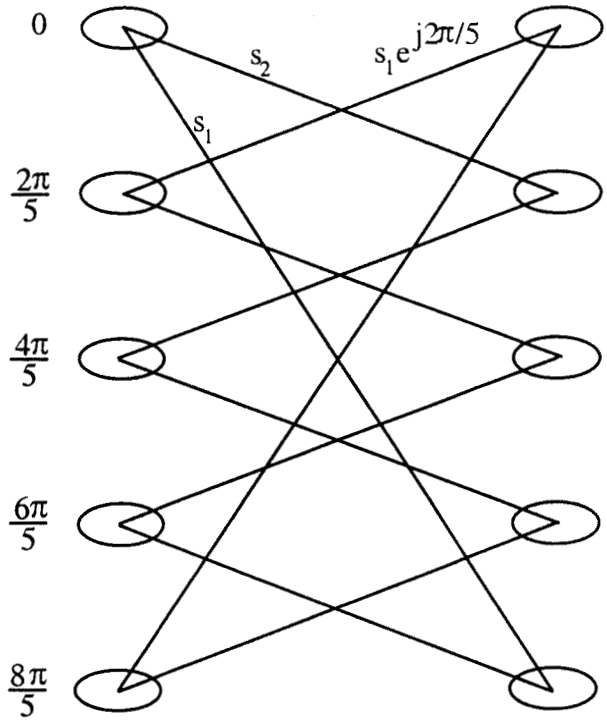

Figure 1-a: The coherent trellis of $h = 2/5$ binary CPFSK, $s_1(t) = 1/\sqrt{T_s} e^{-j\frac{2\pi}{5}\frac{t}{T_s}}$, $s_2(t) = e^{j\frac{2\pi}{5}\frac{t}{T_s}}$.

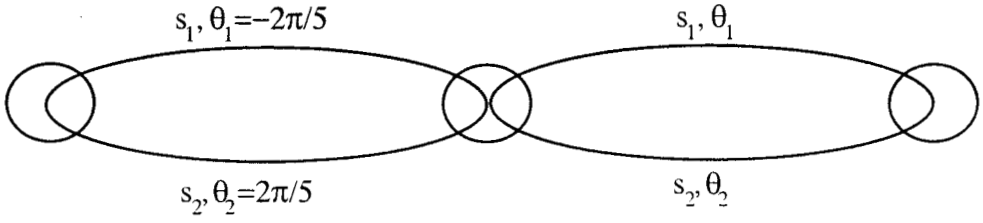

Figure 1-b: The primitive noncoherent trellis of $h = 2/5$ binary CPFSK.

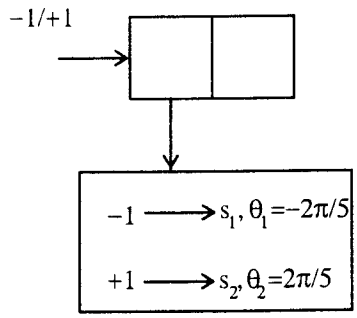

Figure 1-c: The optimal noncoherent encoder of $h = 2/5$ binary CPFSK, $L = 2$. This encoder is not used for encoding, but as a model to build the decoder trellis shown in Fig. 8.1d.

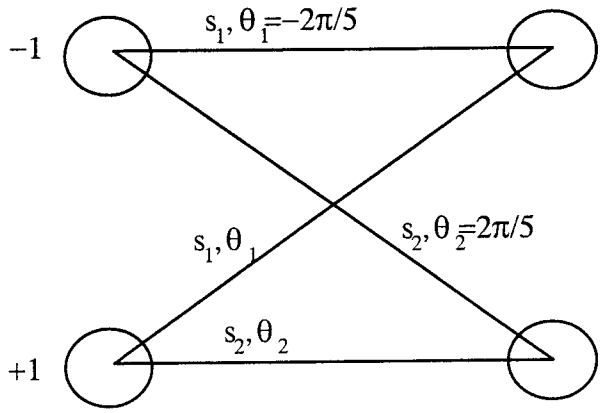

Figure 1-d: The optimal noncoherent trellis of $h = 2/5$ binary CPFSK, $L = 2$.

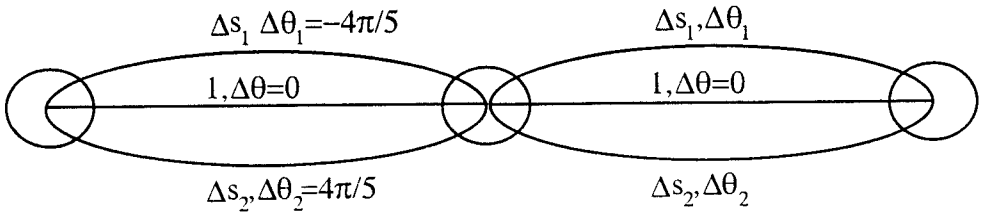

Figure 1-e: The symbol-difference primitive noncoherent trellis of $h = 2/5$ binary CPFSK, $\Delta s_1(t) = e^{-j\frac{4\pi}{5}\frac{t}{T_s}}$, $\Delta s_2(t) = e^{j\frac{4\pi}{5}\frac{t}{T_s}}$.

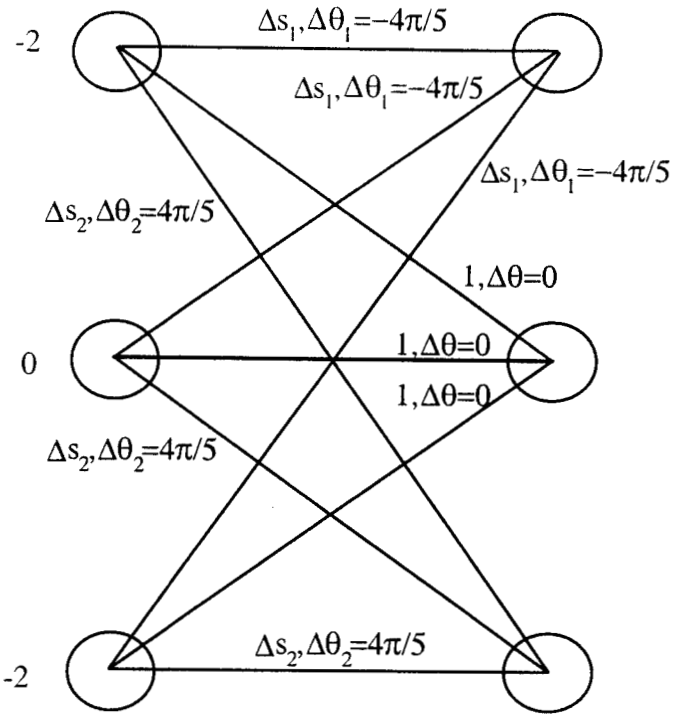

Figure 1-f: The symbol-difference optimal noncoherent trellis of $h = 2/5$ binary CPFSK, $L = 2$.

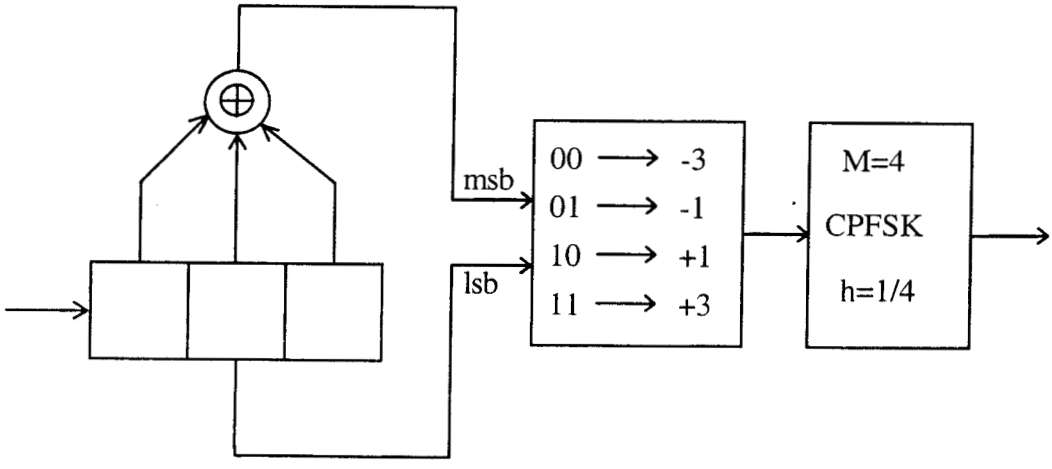

Figure 2: A coded CPFSK encoder, coherent detection.

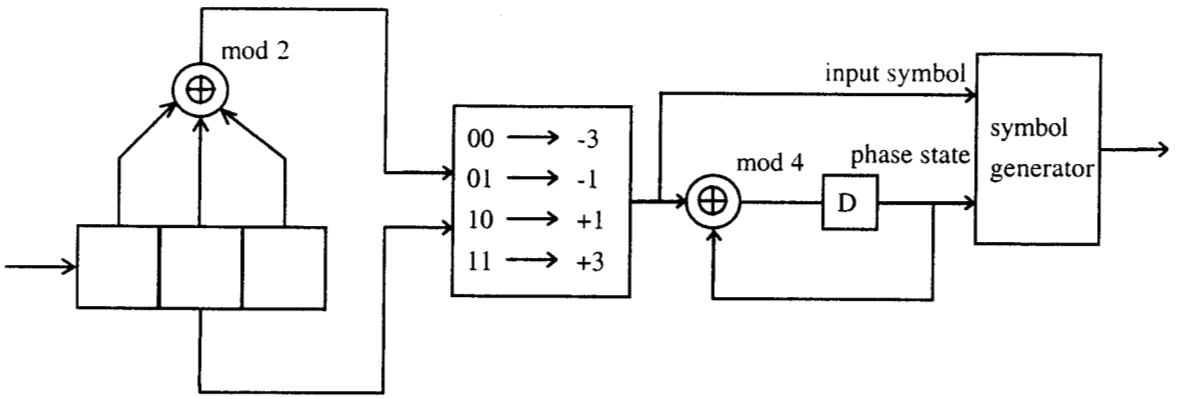

Figure 3: Equivalent encoder of the system of Figure 2, coherent detection.

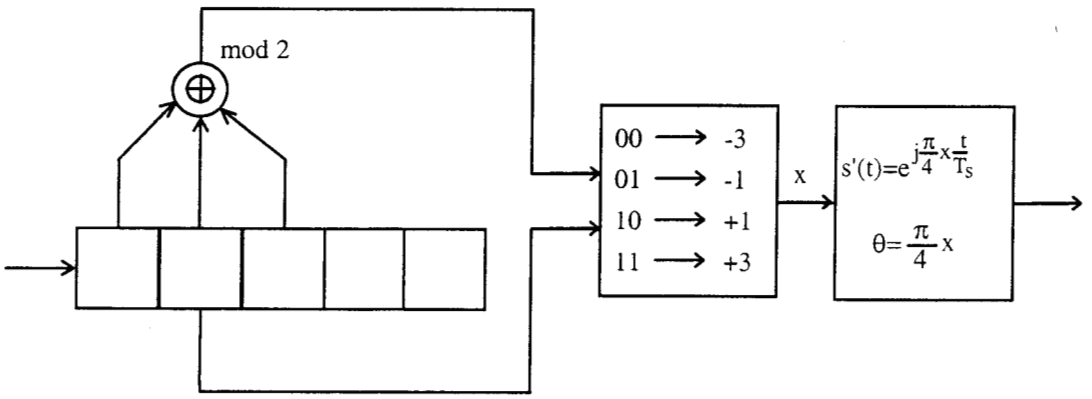

Figure 4: Equivalent encoder of the system of Figure 2, noncoherent detection with $L = 3$.

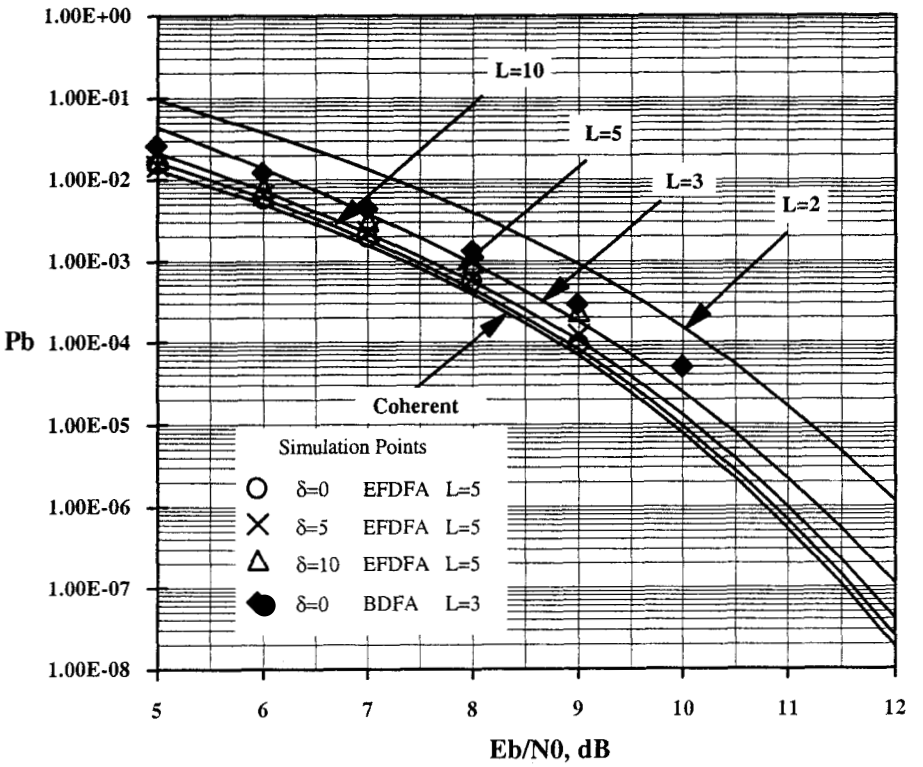

Figure 5: Noncoherent decoding performance of MSK.

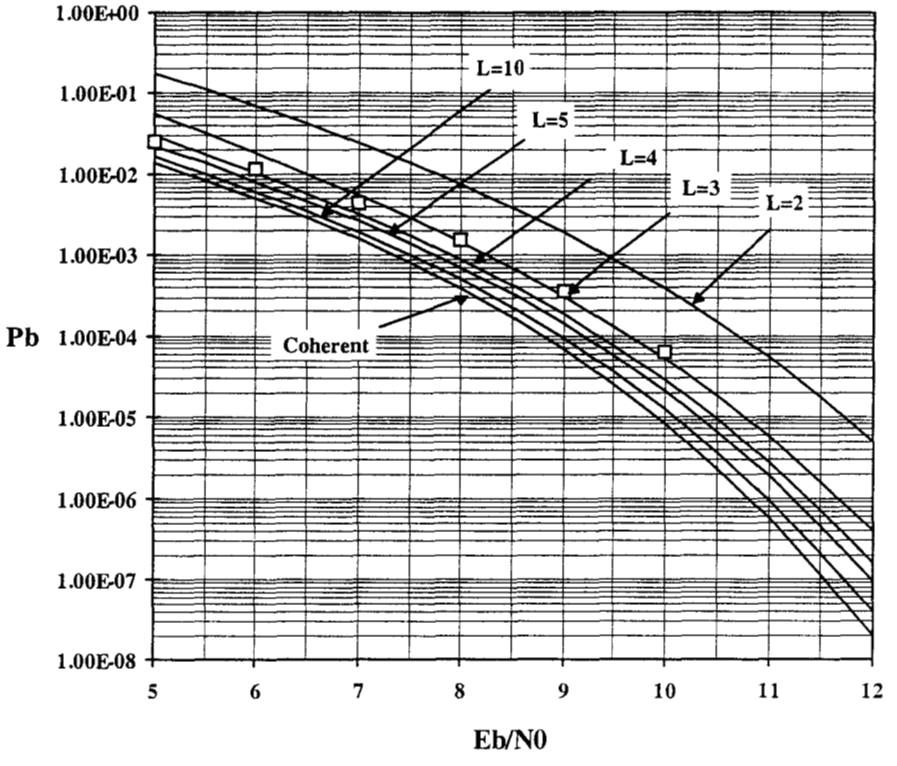

Figure 6: Noncoherent decoding performance of GMSK, $BT = 0.5$. Simulation points with $L = 3$, EFDFA, $\delta = 0$.

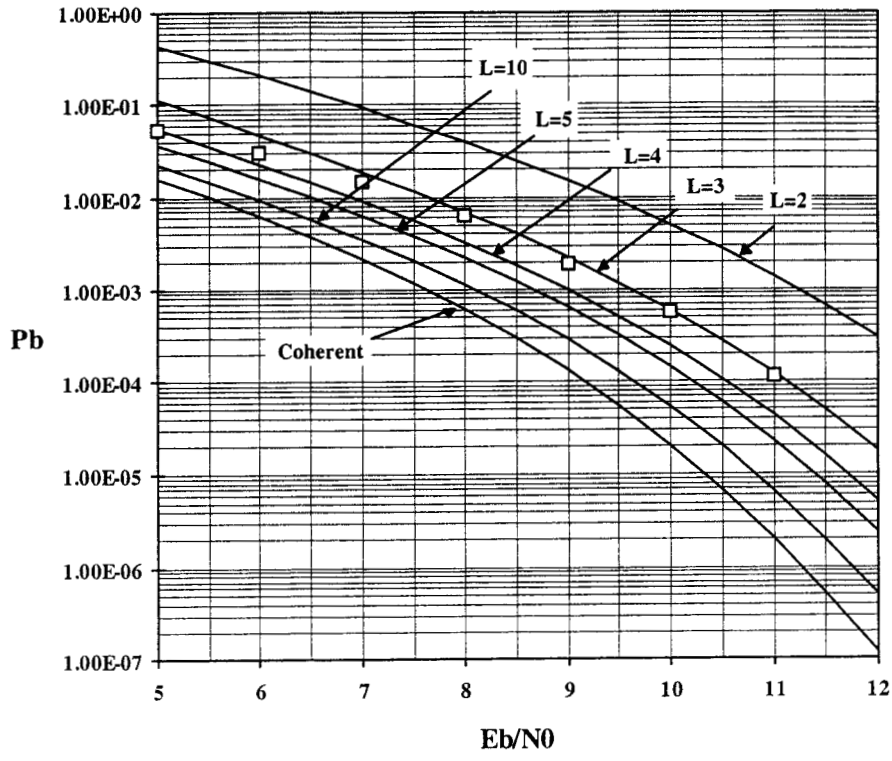

Figure 7: Noncoherent decoding performance of GMSK, $BT = 0.25$. Simulation points with $L = 3$, EFDFA, $\delta = 0$.

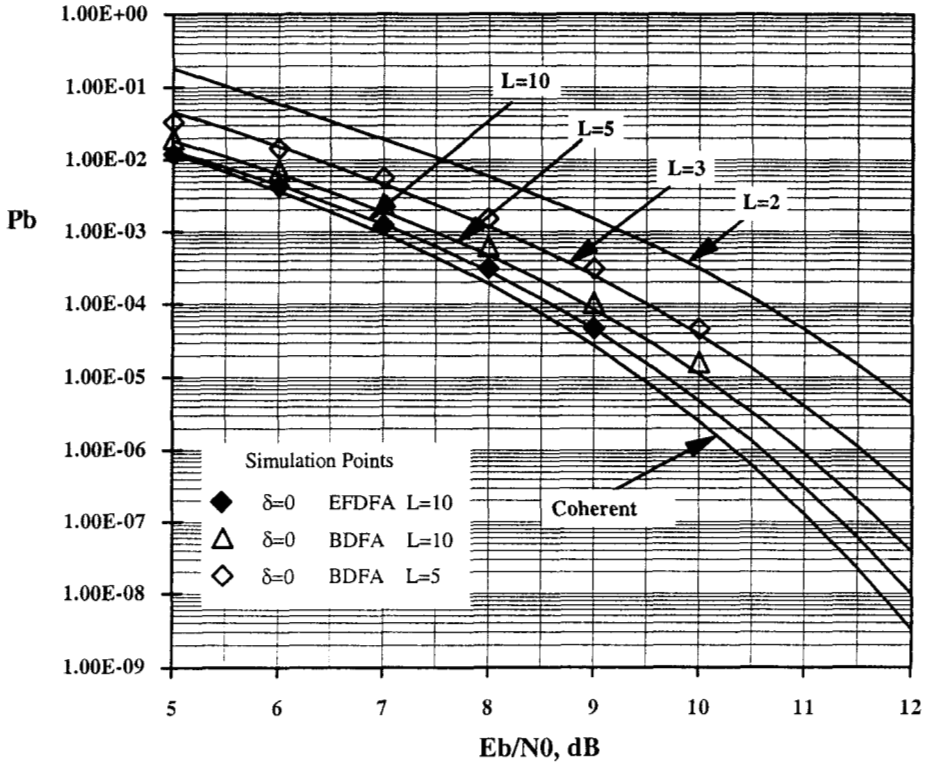

Figure 8: Noncoherent decoding performance of 2RC, $h = 1/3$, 4-level CPM.

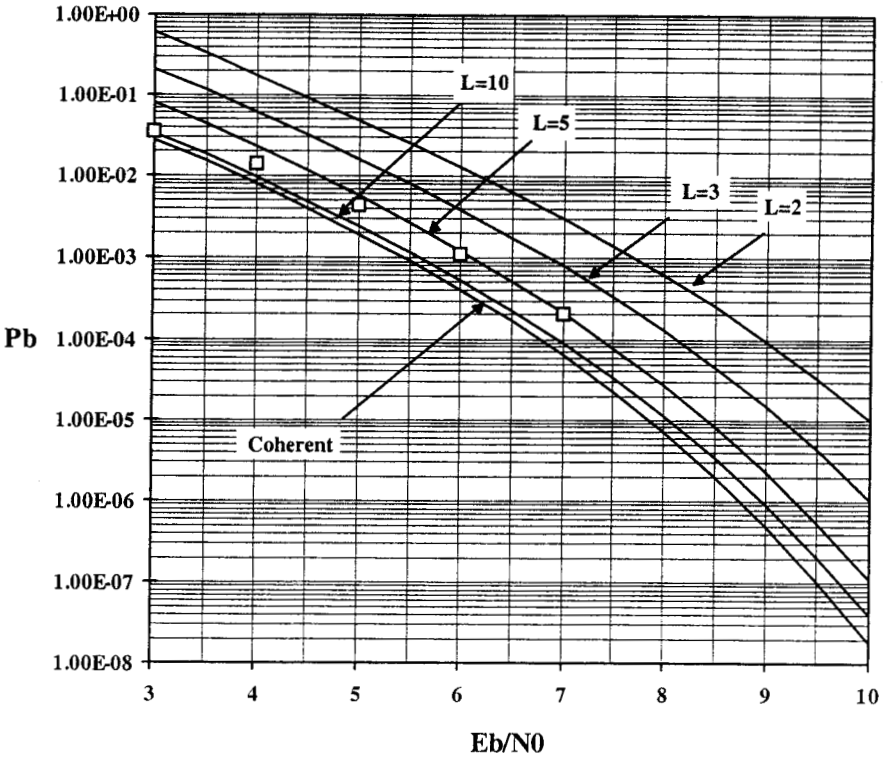

Figure 9: Noncoherent decoding performance of 1REC (CPFSK), $h = 2/5$, 4-level CPM. Simulation points with $L = 5$, EFDFA, $\delta = 0$.

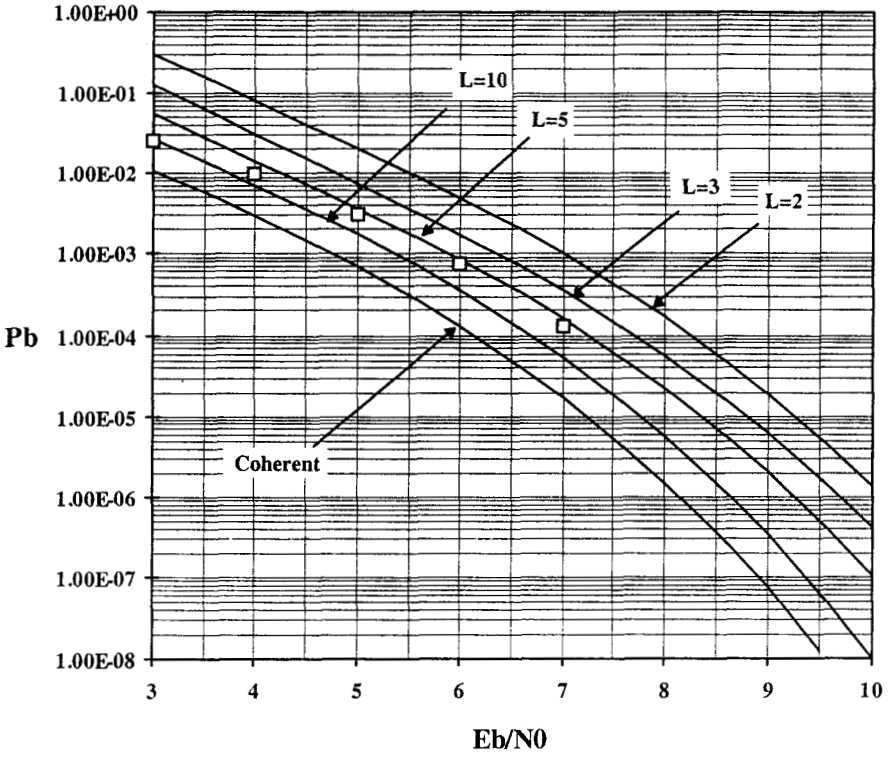

Figure 10: Noncoherent decoding performance of 1REC (CPFSK), $h = 4/9$, 4-level CPM. Simulation points with $L = 5$, EFDFA, $\delta = 0$.

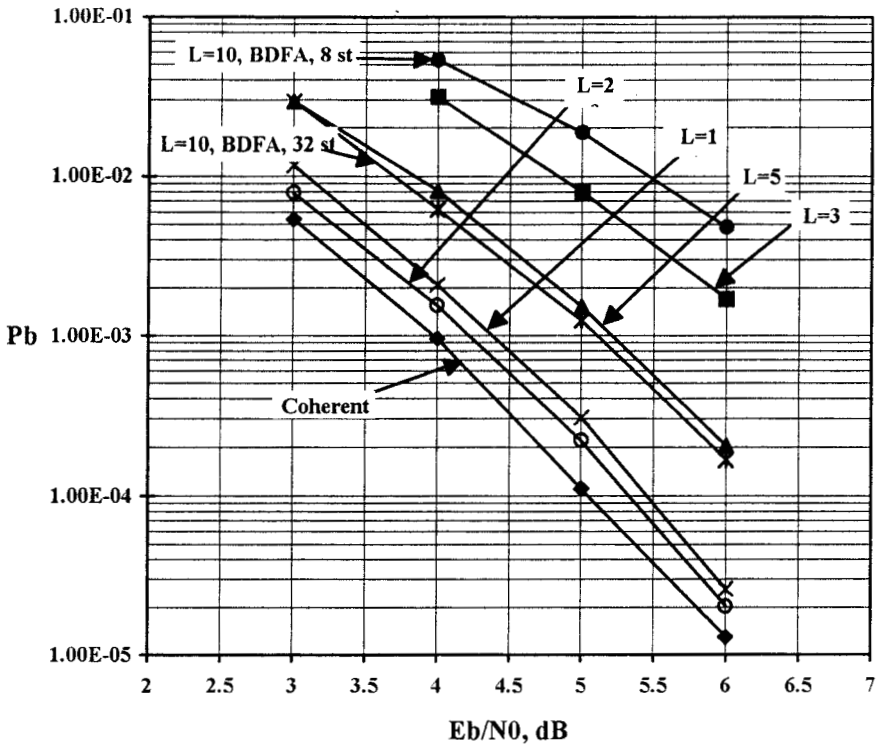

Figure 11: Simulation results of coded CPM with coherent and noncoherent detection. A 4 states binary rate 1/2 code is used with $h = 1/4$ 4-level CPFSK. The encoder is shown in Figure 2. Unless marked differently, simulation with EFDFA, $\delta = 0$.